Article ID: 1000-324X(2023)03-0329-06 **DOI:** 10.15541/jim20220646

Large-size Er,Yb:YAG Single Crystal: Growth and Performance

WANG Zhiqiang[1], WU Ji'an[1], CHEN Kunfeng[1], XUE Dongfeng[2]

(1. Institute of Novel Semiconductors, State Key Laboratory of Crystal Materials, Shandong University, Jinan 250100, China; 2. Multiscale Crystal Materials Research Center, Shenzhen Institute of Advanced Technology, Chinese Academy of Sciences, Shenzhen 518055, China)

Abstract: Currently, although Er^{3+} and Yb^{3+} co-doped YAG crystals are widely used in high power solid state lasers, there are still many challenges in growing large size, low defect doped YAG crystals using the Czochralski (Cz) method. In this paper, large-sized Er^{3+} and Yb^{3+} co-doped YAG bulk crystal with a diameter of 80 mm and a length of 230 mm was obtained by the fast Cz growth method. Their structure, doping concentration, optical absorption, luminescence performances, and etching defects were evaluated.According to the Raman detecting results, there is no significant variation in the peak positions and full width at half maxima (FWHM) of the Raman peaks at different locations on the wafer, indicating that the crystal structure and strain at central and edge section of thel wafer are uniformity. The etching results show that the corrosion pits are evenly distributed over the entire corrosion surfacewithout dislocation corrosion pit, which means that the crystals are highly near perfect. Strong luminescence peaks of Yb^{3+} and Er^{3+} at different wavelengths and glow discharge mass spectrometry results demonstrate the successful doping of rare earth ions in Er,Yb:YAG single crystals. This work successfully used the Cz method to grow large-sized, low-defect Er,Yb:YAG single crystals, confirming that the fast growth method is effective for doping double rare-earth ions in YAG crystals.

Key words: YAG single crystal; rare earth doping; fast Cz growth method; luminescence property

Yttrium aluminium garnet ($Y_3Al_5O_{12}$, YAG) is important host material for phosphors, scintillators, and solid state lasers[1-3]. With the valence 4f electrons shield by 5s and 5p electron orbits, the rare earth ions in the solid state often emit in narrow and strong bands[4]. The rare earths of most interest for selective emitters are ytterbium (Yb), thulium (Tm), erbium (Er), holmium (Ho) and dysprosium (Dy). Rare earth doped YAG crystal have been used in photonic applications ranging from near infrared (IR) emitters to cathode ray phosphors and scintillators since Y^{3+} being vicariate with trivalent lanthanide ions[5]. Yb^{3+} ions can absorb the light between 900 and 1000 nm with energy transfer (ET) from $^2F_{7/2}$ to $^2F_{5/2}$ level. Then, the energy can be transferred to the $^4I_{11/2}$ level of Er^{3+}, leading to laser emission at 2.94 μm wavelength. Therefore, Er and Yb doped glass, ceramics, fiber and single crystal materials have been synthesized for studying up-conversion luminescence and active lasing performances[6-10]. Er^{3+},Yb^{3+}: YAG crystals of a diameter of about 25 mm and a length of 60 mm were obtained using Cz method[7]. It was reported that 8 inch (20.32 cm) Yb:YAG single crystal was grown by Cz method[8]. The Er^{3+}/Yb^{3+} co-doped YAG fiber (about 3 mm in length and 0.8 mm in cross section diameter) have been grown by laser heated pedestal growth[9]. Recently, Er,Yb co-doped YAG single crystals (70 mm×150 mm×15 mm) was grown by a modified horizontal directional crystallization method in Ar+(CO, H_2) atmosphere using Mo crucible[11]. The growth of larger size of Er,Yb co-doped YAG single-crystals was still in demand.

However, it is a challenge to grow bulk YAG single crystals with low defects. We have used the chemical bonding theory of single crystal growth quantitatively to describe the anisotropic bonding behaviors of constituent atoms during YAG crystallizing, and ϕ3 inch(1 inch=2.54 mm) YAG crystal were obtained[12-13]. In this work, we grew

Received date: 2022-11-01; **Revised date:** 2022-11-30; **Published online:** 2023-01-17
Foundation item: National Natural Science Foundation of China (51832007, 52220105010); Natural Science Foundation of Shandong Province (ZR2020ZD35); Qilu Young Scholars Program of Shandong University
Biography: WANG Zhiqiang (1998–), male, Master. E-mail: wangzhiqiang@mail.sdu.edu.cn
王志强(1998–), 男, 硕士. E-mail: wangzhiqiang@mail.sdu.edu.cn
Corresponding author: CHEN Kunfeng, professor. E-mail: Kunfeng.Chen@sdu.edu.cn; XUE Dongfeng, professor. E-mail: df.xue@siat.ac.cn
陈昆峰, 教授. E-mail: Kunfeng.Chen@sdu.edu.cn; 薛冬峰, 教授. E-mail: df.xue@siat.ac.cn

Er,Yb:YAG single crystal with a diameter of 80 mm and length of 230 mm with fast growth method. The structure, defect, optical and luminescence performances were studied.

1 Experimental

1.1 Er,Yb:YAG crystal growth

The Er,Yb:YAG polycrystals were synthesized with the powders of Er_2O_3 (99.999%), Yb_2O_3 (99.999%), Y_2O_3 (99.999%) and Al_2O_3 (99.999%) as raw materials. First, all ingredients were dried to remove residual moisture from the powder to ensure accurate weighing. The doping concentrations of Yb^{3+} and Er^{3+} were 0.05% and 0.15% (in mass), respectively. The four powders were mixed and blended in a mixer for 24 h to ensure that the ingredients were well mixed. The mixed powders were then packed into a mould and compacted. Finally, the pressed cylinders were transferred to a muffle furnace and sintered at 1100 ℃ for 12 h to form polycrystalline Er,Yb:YAG.

The growth of Er,Yb:YAG single crystal was carried out by the Cz method in a nitrogen atmosphere. The sintered polycrystalline Er,Yb:YAG was put into an iridium crucible equipped with an intermediate frequency induction heating system Cz furnace, heated until the polycrystalline material is completely melted and held for a period. The YAG in the <111> direction was used as the seed crystal and seeding was performed manually. A series of subsequent crystal growth processes were controlled by an automatic control system with the following specific growth parameters: a pulling rate of 2–4 $mm \cdot h^{-1}$ and rotation rate of 5–10 r/min[12].

1.2 Characterization

The crystal phase of single crystal Er,Yb:YAG were examined with X-ray diffraction (XRD, Rigaku, Smartlab 3kW). The elemental analysis of the Er,Yb:YAG crystal was characterized by Energy-dispersive X-ray spectroscopy (EDS, Oxford, Ultim Max 100) and glow discharge mass spectrometry (GDMS, AstruM, Nu Instrument). Raman spectra were excited using Raman spectrometer (Horiba, LabRAM HR Evolution) with a 325 nm laser. Etched Er,Yb:YAG wafers were performed by optical microscope (Nikon, LV150). The refractive index of Er,Yb:YAG wafer was measured by Prism Coupling device (Metricon, Model 2010). The optical absorption and PL spectra were determined by UV-Vis spectrophotometer (Metash, UV-9000) and fluorescence spectrometer (Edinburgh, FLS 1000), respectively.

2 Results and discussion

Fig. 1(a) shows the photograph of a large-size Er,Yb:YAG single crystal grown by the Cz method and annealed in air. Fig. 1(b) shows the picture of a wafer with a thickness of 1.5 mm cut perpendicular to the orientation of <111> and polished on both sides. The length and diameter of the crystal are 230 and 80 mm, respectively. The shape is characteristic of typical <111> orientation, and the crystal is colourless transparent and has no defects such as cracks and inclusions[14-15].

Grind the annealed crystal into powder for XRD analysis, and the results are shown in Fig. 1(c). A comparison of the XRD results with the standard PDF cards (PDF# 00-033-0040) in the database shows that all peaks are well indexed to the cubic structure $Y_3Al_5O_{12}$ (space group: $Ia\bar{3}d$), and no impurity phases are found, which means that the dopant ions are well substituted for the Y^{3+} lattice positions[16-17]. XRD tests on the YAG-doped wafer in Fig. 1(b) show only a sharp diffraction peak of the (444) crystal plane at 2θ=52.76° and no diffraction peaks of the other crystal planes, confirming its good quality.

The chemical compositions of Er,Yb:YAG crystal were determined by EDS and GDMS. It can be seen in Fig. 1(d) that Y, Al and O peaks are well detected. Because the element contents of Yb and Er are relatively low, and the characteristic energies of these elements are located at 1.521 and 1.405 keV, which are close to the peaks of Al (1.486 keV) and overlap, they cannot be distinguished well. GDMS is one of the effective means of analysing trace elements in conductors and semiconductors[18-19]. The actual doping concentrations of Er^{3+} and Yb^{3+} ions in YAG crystals were analysed using GDMS. The results showed that the actual doping content of Er^{3+} and Yb^{3+} was 0.13% and 0.049% (in mass), demonstrating the successful doping of Er^{3+} and Yb^{3+}.

In order to study the defects present in the grown Er,Yb:YAG crystal, the polished wafers were chemically etched. The etching was carried out using concentrated phosphoric acid (H_3PO_4) at 180 ℃ for 60 min. A comparison of the wafer surface before and after corrosion is shown in Fig. 2. The corrosion pits are evenly distributed over the entire corrosion surface, and no dislocation corrosion pit features are observed, which means that the crystals are near-perfect[20-21].

For cubic $Y_3Al_5O_{12}$ (YAG) with space group $O_h^{10} - Ia\bar{3}d$, the irreducible representations as follows: $\Gamma = 3A_{1g} + 5A_{2g} + 5A_{1u} + 5A_{2u} + 8E_g + 10E_u + 14T_{1g} + 14T_{2g} +$

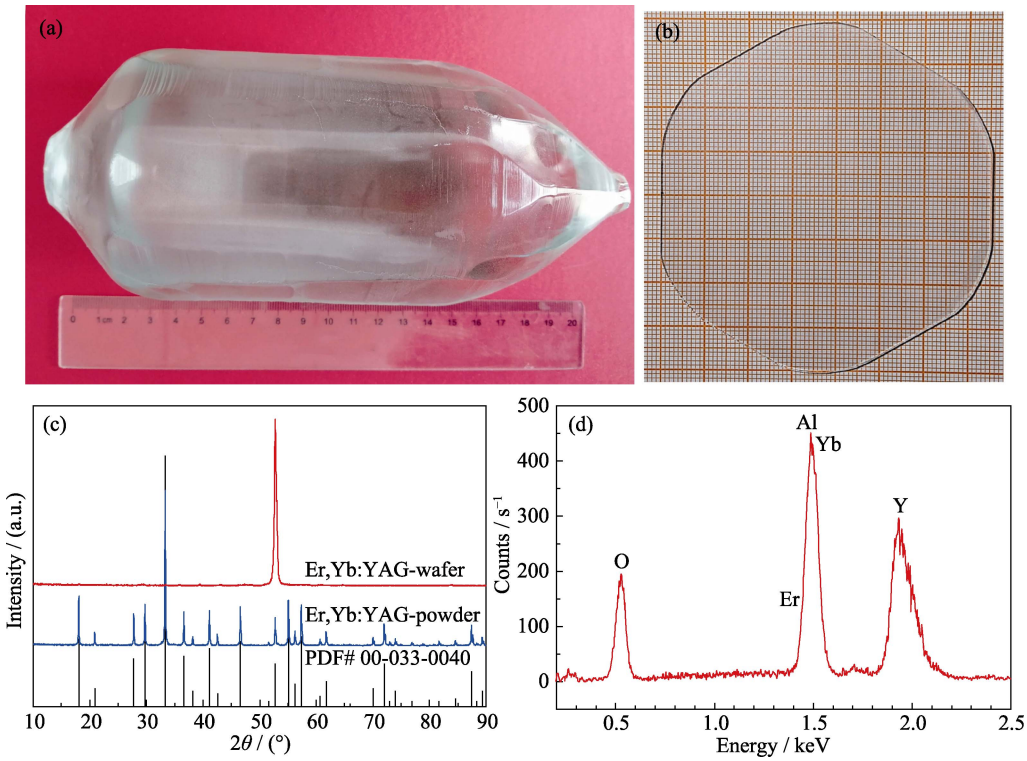

Fig. 1　Characteristics of as-grown Er,Yb:YAG single crystal and wafer
(a) With diameter of 80 mm and length of 230 mm; (b) Wafer with a thickness of 1.5 mm;
(c) XRD patterns for wafer and ground powder; (d) EDS pattern of the wafer

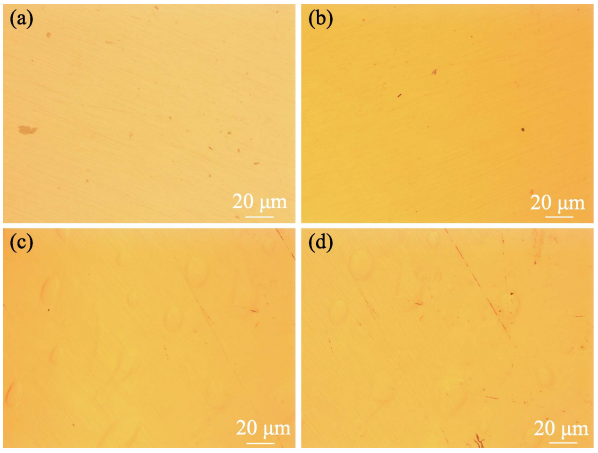

Fig. 2　Micrographs of wafer surface with (111) face
(a, b) Before etching; (c, d) Etched in H_3PO_4 at 180 ℃ for 60 min

$18T_{1u}$ + $16T_{2u}$. 25 modes are Raman active ($3A_{1g}$, $8E_g$ and $14T_{2g}$) while 18 modes are IR active ($18T_{1u}$)[22]. The Raman spectra of rare earth doped YAG have been recorded in the 100–1200 cm^{-1} spectral range at room temperature (Fig. 3 and Fig. 4(a)), which shows strong Raman bands at 259, 371, 402, 784 cm^{-1}, medium bands at 161, 218, 548, 558, 692, 718, 859 cm^{-1}, and weak bands at 294, 338, 754 cm^{-1}. The low-frequency region (100–500 cm^{-1}) can be attributed to the lattice vibrational mode and the translational motion of the RE^{3+}(Y,Er,Yb), and also the mixing of translational, rotational and ν_3 molecular mode of the [AlO_4] unit. The intermediate-frequency region (500–600 cm^{-1}) accounts to the ν_2 molecular mode splitting of the [AlO_4] unit while the high-frequency region (600–900 cm^{-1}) can be assigned to the ν_1 and ν_4 internal modes of the tetrahedral [AlO_4] unit[23-24]. According to the results of factor group analysis, the three A_{1g} modes are related to the [AlO_4] internal vibrations[25]. There is a weak Raman peak at 1100 cm^{-1}, which may be the Yb–O vibration[26-27]. To investigate the doping uniformity of Er,Yb:YAG crystal grown by the Cz method, two sets of points were taken outside the center of the wafer (the inset of Fig. 4(b)). Raman spectra of these points showed that the peak

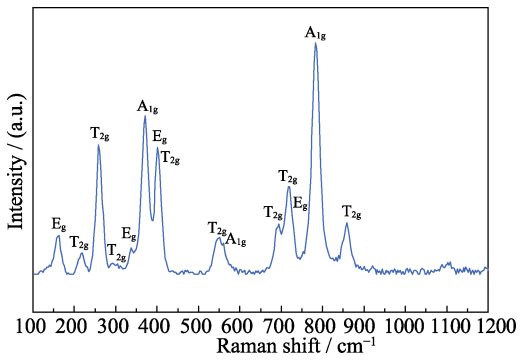

Fig. 3　Raman spectrum of Er,Yb:YAG

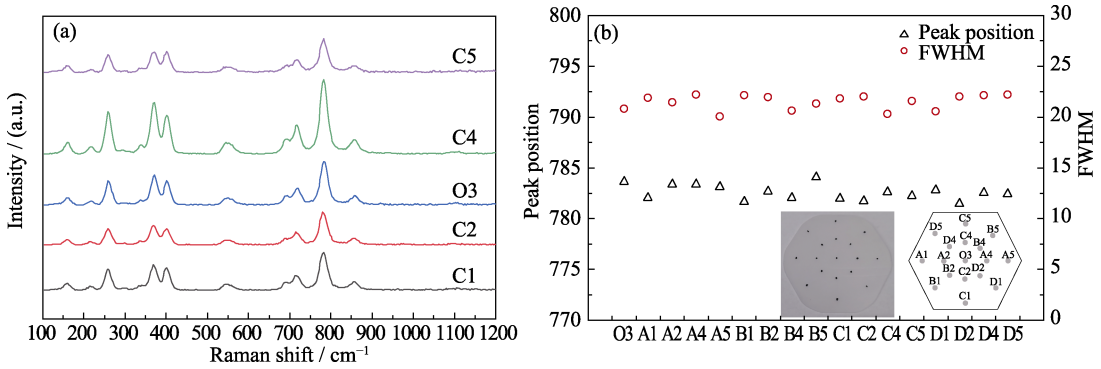

Fig. 4 Raman spectra of different points at Er,Yb:YAG wafer

(a) Five points on a straight line; (b) Peak positions and FWHM obtained by Lorentz fitting at the 783 cm^{-1} band with nisets showing Er,Yb:YAG wafer and schematic diagram of Raman test points

intensity of the C4 point is the highest at the 783 cm^{-1} band. Raman spectra of other points are similar to those of C1, C2 and O3 (Fig. 4(a)). Lorentz fitting was performed on all selected points at the 783 cm^{-1} band (Fig. 4(b)).

The peak position obtained by B5 point fitting is 784 cm^{-1}, which means that B5 point is subjected to higher compressive stress than other points. The peak position varies from 781.5 to 784.1 cm^{-1}, and FWHM varies from 20 to 22.2 cm^{-1}. The peak position and FWHM of each point were not greatly changed. Therefore, it can be considered that the doping uniformity of the wafer is relatively acceptable.

The room-temperature UV-Vis absorption spectra in 200–1050 nm of Er,Yb:YAG in Fig. 1(b) are shown in Fig. 5. The absorption bands centered at 914 and 941 nm are attributed to the transitions from the ground state to the excited state ($^2F_{7/2}\rightarrow{}^2F_{5/2}$) of Yb^{3+} ion[11, 28-29]. It can be seen from the illustration in Fig. 5 that Er,Yb:YAG crystal has strong UV absorption band when the wavelength less than 230 nm, which is caused by charge transfer (CT) luminescence from O^{2-} to Yb^{3+}[30-31]. Except for the optical absorption of Yb^{3+} and CT luminescence,

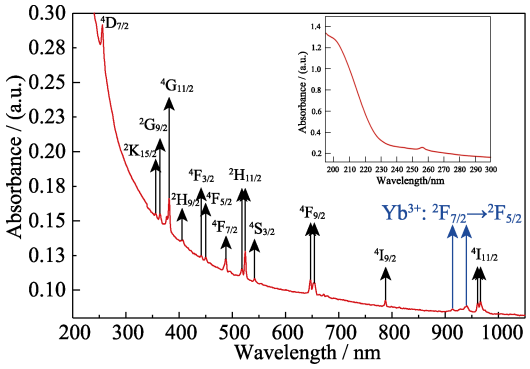

Fig. 5 Optical absorption spectra of Er,Yb:YAG crystal in the range of 200–1050 nm at room temperature

Table 1 Correspondence between the experimentally observed absorption lines and energy levels of Er^{3+} in Er,Yb:YAG single crystal[11, 33-36]

Wavelength/nm	Assignment (from ground $^4I_{15/2}$)
255	$^4D_{7/2}$
356	$^2K_{15/2}$
364	$^2G_{9/2}$
381	$^4G_{11/2}$
407	$^2H_{9/2}$
442	$^4F_{3/2}$
450	$^4F_{5/2}$
488	$^4F_{7/2}$
518, 524	$^2H_{11/2}$
542	$^4S_{3/2}$
647, 655	$^4F_{9/2}$
788	$^4I_{9/2}$
961, 966	$^4I_{11/2}$

all remaining peaks in the absorption spectra are attributed to the transitions of Er^{3+} ion[11, 32]. The assignment of the absorption lines of the Er^{3+} ion is presented in Table 1. The refraction index of Er,Yb:YAG is 1.83.

Fig. 6 illustrates the emission spectra of crystals excited at different wavelengths at room temperature, 382 nm for Fig. 6(a) and 260 nm for Fig. 6(b). It can be seen from Fig. 6(a) that the green emission at 554 nm has the strongest emission peak, which corresponds to the $^4S_{3/2}\rightarrow{}^4I_{15/2}$ energy levels transition in Er^{3+} ion[37]. The violet emission at 405 nm shown in Fig. 6(b) is attributed to the $^2H_{9/2}\rightarrow{}^4I_{15/2}$ in Er^{3+} ion[38]. The decay curves of the fluorescence lifetimes of the emission peaks at 554 and 405 nm are presented in Fig. 6(c, d). The fitting results show that the fluorescence lifetimes are 17.92 and 52.09 μs, respectively.

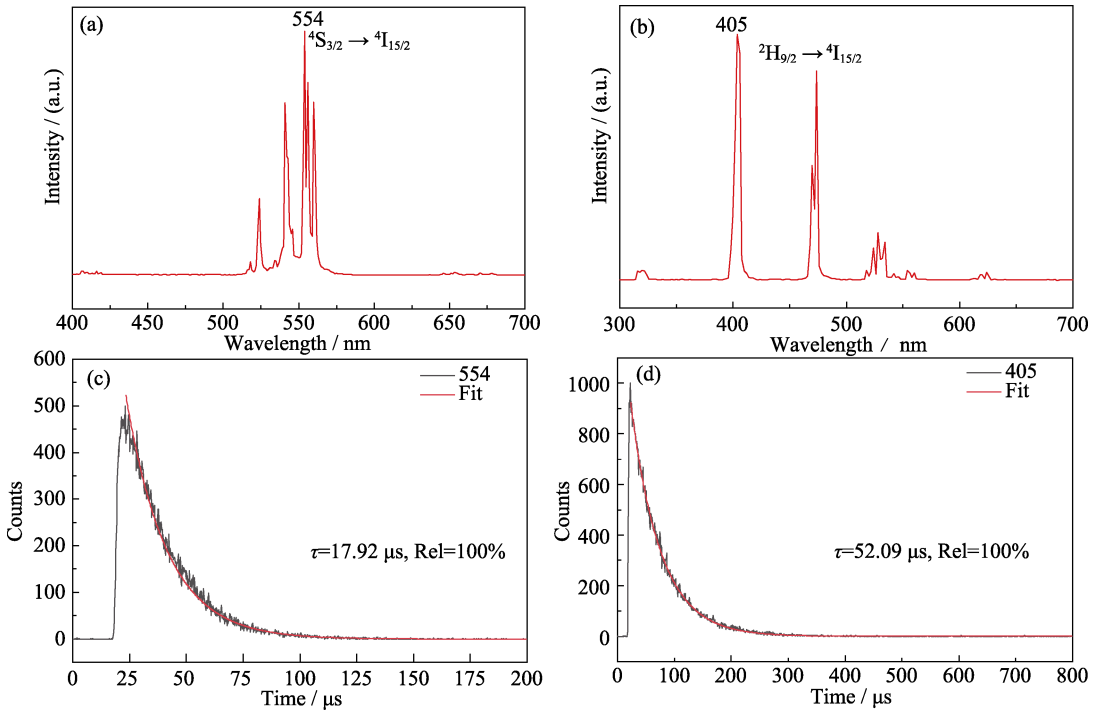

Fig. 6　Emission spectra of Er,Yb:YAG crystal at room temperature

(a) Excited by 382 nm; (b) Excited by 260 nm; Fluorescent decay curves of (c) 554 nm; (d) 405 nm emission; Colorful figures are available on website

3　Conclusion

In this work, cubic-phase Er,Yb:$Y_3Al_5O_{12}$ crystal with a diameter of 80 mm and length of 230 mm was obtained by the fast Cz growth method. Raman results of 17 points in cutting crystal wafer showed uniform peak number and position, which can be considered that the structure uniformity of the wafer is relatively acceptable. The refraction index of Er,Yb:YAG is 1.83. The absorption bands are attributed to the transitions from the ground state to the excited state of Yb^{3+} and Er^{3+} ions. Expect for the optical absorption of Yb^{3+} and CT luminescence, all remaining narrow peaks in the absorption spectra are attributed to the transitions of Er^{3+} ion. It is concluded that the fast growth method was effective for dual rare earth ions doping in YAG crystal.

References:

[1] MA X G, LI X Y, LI J Q, *et al*. Pressureless glass crystallization of transparent yttrium aluminum garnet-based nanoceramics. *Nature Communications*, 2018, **9(1):** 1175.

[2] SUN C T, XUE D. Study on the crystallization process of function inorganic crystal materials. *Scientia Sinica Technologica*, 2014, **44(11):** 1123.

[3] SUN C T, XUE D. Chemical bonding in micro-pulling down process: high throughput single crystal growth. *Science China Technological Sciences*, 2018, **61(11):** 1776.

[4] CHUBB D L, PAL A M T, PATTON M O, *et al*. Rare earth doped yttrium aluminum garnet (YAG) selective emitters. *Materials & Design*, 2001, **22(7):** 591.

[5] UPASANI M, BUTEY B, MOHARIL S V. Photoluminescence study of rare earth doped yttrium aluminum garnet-YAG:RE (RE: Eu^{3+}, Pr^{3+} and Tb^{3+}). *Optik*, 2016, **127(4):** 2004.

[6] GEORGIOU E, MUSSET O, BOQUILLON J P, *et al*. 50 mJ/30 ns FTIR Q-switched diode-pumped Er:Yb:glass 1.54 μm laser. *Optics Communications*, 2001, **198(1/2/3):** 147.

[7] MIERCZYK Z, KWASNY M, KOPCZYNSKI K, *et al*. Er^{3+} and Yb^{3+} doped active media for 'Eye-Safe' laser systems. *Journal of Alloys and Compounds* 2020, **300(1):** 398.

[8] YANG G, HAN J, LI X, *et al*. Growth of 8 inch Yb:YAG single crystal by Czochralski method. *Journal of Synthetic Crystals*, 2019, **48:** 1216.

[9] BAO R J, YU L, YE L H, *et al*. Compact and sensitive Er^{3+}/Yb^{3+} co-doped YAG single crystal optical fiber thermometry based on up-conversion luminescence. *Sensors and Actuators A: Physical*, 2018, **269:** 182.

[10] GUO Y, HUANG L, ZHOU J, *et al*. Czochralski growth and investigation on the photoluminescence properties of YAG:Er single crystal. *Journal of Synthetic Crystals*, 2019, **48:** 24.

[11] NIZHANKOVSKYI S V, KOZLOVSKYI A A, KOVALENKO N O, *et al*. Optical and luminescence properties of Er,Yb:YAG crystals grown by horizontal directional crystallization method. *Functional Materials*, 2019, **26(1):** 35.

[12] SUN C T, XUE D. Chemical bonding theory of single crystal growth and its application to ϕ3" YAG bulk crystal. *CrystEngComm*, 2014, **16(11):** 2129.

[13] SUN C T, XUE D. Crystal growth: an anisotropic mass transfer process at the interface. *Physical Chemistry Chemical Physics*, 2017, **19(19):** 12407.

[14] YANG P Z, DENG P Z, XU J, *et al*. Growth of high-quality single crystal of 30at% Yb:YAG and its laser performance. *Journal of Crystal Growth*, 2000, **216(1–4):** 348.

[15] XU X D, ZHAO Z W, SONG P X, *et al*. Growth of high-quality single crystal of 50at% Yb:YAG and its spectral properties.

Journal of Alloys and Compounds, 2004, **364(1/2):** 311.
[16] XU X D, ZHAO Z W, WANG H H, *et al*. Spectroscopic and thermal properties of Cr,Yb:YAG crystal. *Journal of Crystal Growth*, 2004, **262(1–4):** 317.
[17] ZHU M D, QI H J, PAN M Y, *et al*. Growth and luminescent properties of Yb:YAG and Ca co-doped Yb:YAG ultrafast scintillation crystals. *Journal of Crystal Growth*, 2018, **490:** 51.
[18] BOGAERTS A, GIJBELS R. New developments and applications in GDMS. *Fresenius Journal of Analytical Chemistry*, 1999, **364(5):** 367.
[19] DI SABATINO M. Detection limits for glow discharge mass spectrometry (GDMS) analyses of impurities in solar cell silicon. *Measurement*, 2014, **50:** 135.
[20] YANG P Z, DENG P Z, YIN Z W, *et al*. The growth defects in Czochralski-grown Yb:YAG crystal. *Journal of Crystal Growth*, 2000, **218(1):** 87.
[21] YIN H B, DENG P Z, GAN F X. Defects in YAG:Yb crystals. *Journal of Applied Physics*, 1998, **83(7):** 3825.
[22] HURRELL J P, PORTO S P S, CHANG I F, *et al*. Optical phonons of yttrium aluminum garnet. *Physical Review*, 1968, **173(3):** 851.
[23] PAPAGELIS K, KANELLIS G, VES S, *et al*. Lattice dynamical properties of the rare earth aluminum garnets ($RE_3Al_5O_{12}$). *Physica Status Solidi B-Basic Solid State Physics*, 2002, **233(1):** 134.
[24] CHEN Y F, LIM P K, LIM S J, *et al*. Raman scattering investigation of Yb:YAG crystals grown by the Czochralski method. *Journal of Raman Spectroscopy*, 2003, **34(11):** 882.
[25] PAPAGELIS K, KANELLIS G, ARVANITIDIS J, *et al*. Phonons in rare-earth aluminum garnets and their relation to lattice vibration of AlO_4. *Physica Status Solidi B-Basic Research*, 1999, **215(1):** 193.
[26] QIU H W, YANG P Z, DONG J, *et al*. The influence of Yb concentration on laser crystal Yb:YAG. *Materials Letters*, 2002, **55(1/2):** 1.
[27] WANG T, ZHANG J, ZHANG N, *et al*. The characteristics of high-quality Yb:YAG single crystal fibers grown by a LHPG method and the effects of their discoloration. *RSC Advances*, 2019, **9(39):** 22567.
[28] WANG X D, XU X D, ZENG X H, *et al*. Effects of Yb concentration on the spectroscopic properties of Yb:$Y_3Al_5O_{12}$. *Spectrochimica Acta Part A-Molecular and Biomolecular Spectroscopy*, 2006, **63(1):** 49.
[29] WANG X D, XU X D, ZHAO Z W, *et al*. Comparison of fluorescence spectra of Yb:$Y_3Al_5O_{12}$ and Yb:$YAlO_3$ single crystals. *Optical Materials*, 2007, **29(12):** 1662.
[30] GUERASSIMOVA N, GARNIER N, DUJARDIN C, *et al*. X-ray-excited charge transfer luminescence in YAG:Yb and YbAG. *Journal of Luminescence*, 2001, **94:** 11.
[31] ZORENKO Y, GORBENKO V, SAVCHYN V, *et al*. Luminescence properties and energy transfer processes in YAG:Yb,Er single crystalline films. *Radiation Measurements*, 2013, **56:** 134.
[32] SARDAR D K, RUSSELL C C, GRUBER J B, *et al*. Absorption intensities and emission cross sections of principal intermanifold and inter-stark transitions of Er^{3+} ($4f^{11}$) in polycrystalline ceramic garnet $Y_3Al_5O_{12}$. *Journal of Applied Physics*, 2005, **97(12):** 123501.
[33] BURDICK G W, GRUBER J B, NASH K L, *et al*. Analyses of $4f^{11}$ energy levels and transition intensities between stark levels of Er^{3+} in $Y_3Al_5O_{12}$. *Spectroscopy Letters*, 2010, **43(5):** 406.
[34] ZHOU J, ZHANG W X, WANG L, *et al*. Fabrication, microstructure and optical properties of polycrystalline Er^{3+}:$Y_3Al_5O_{12}$ ceramics. *Ceramics International*, 2011, **37(1):** 119.
[35] SEKITA M, HANEDA H, SHIRASAKI S, *et al*. Optical spectra of undoped and rare‐earth‐(=Pr, Nd, Eu, and Er) doped transparent ceramic $Y_3Al_5O_{12}$. *Journal of Applied Physics*, 1991, **69(6):** 3709.
[36] NIZHANKOVSKYI S V, KOZLOVSKYI A A, KOVALENKO N O, *et al*. Spectral properties of Er-doped yttrium aluminum garnet crystals grown by modified horizontal directional crystallization method. *Functional Materials*, 2018, **25(4):** 646.
[37] BI F, DONG X T, WANG J X, *et al*. Facile electrospinning preparation and up-conversion luminescence performance of $Y_3Al_5O_{12}$:Er^{3+},Yb^{3+} nanobelts. *Journal of Inorganic and Organometallic Polymers and Materials*, 2014, **24(2):** 407.
[38] KATARIA V, MEHTA D S. Investigation of concurrent emissions in visible, UV and NIR region in Gd_2O_2S:Er,Yb nanophosphor by diverse excitation wavelengths as a function of firing temperature. *Optical Materials*, 2019, **95:** 109204.

大尺寸 Er,Yb:YAG 单晶的生长及其性能

王志强[1], 吴济安[1], 陈昆峰[1], 薛冬峰[2]

(1. 山东大学 晶体材料国家重点实验室, 新一代半导体材料研究院, 济南 250100; 2. 中国科学院 深圳先进技术研究院, 多尺度晶体材料研究中心, 深圳 518055)

摘 要: Er^{3+}和 Yb^{3+}共掺杂的 YAG 晶体是一种非常重要的光学晶体, 目前, 该晶体已经广泛应用于高功率固体激光器, 但是采用提拉法生长大尺寸、低缺陷的掺杂 YAG 晶体仍然面临很多挑战。本工作采用快速提拉法成功获得了直径为 80 mm、长度为 230 mm 的 Er^{3+}和 Yb^{3+}共掺杂的 YAG 单晶。采用不同测试方法评价其结构、掺杂浓度、光吸收、发光性能和刻蚀缺陷。晶片不同位置的拉曼峰峰位以及半峰宽没有明显变化, 说明晶片中心和边缘部分的晶体结构和应变是均匀的。刻蚀结果表明, 腐蚀坑均匀分布在整个腐蚀表面上, 没有观察到位错腐蚀坑特征, 这意味着晶体接近完美。Er^{3+}和 Yb^{3+}在不同波长下的强发光峰以及辉光放电质谱结果证明 Er,Yb:YAG 单晶中成功掺杂了稀土离子。本工作采用提拉法成功生长了大尺寸、低缺陷的 Er,Yb:YAG 单晶, 证实了快速生长方法对 YAG 晶体中掺杂双稀土离子是有效的。

关 键 词: YAG 单晶; 稀土掺杂; 快速提拉法; 发光性能

中图分类号: O782 **文献标志码:** A